Numerical exploration of the spiral state in the pattern formation of the Swift-Hohenberg equation on a sphere

Fumitoshi Gotoh[1], Sotos C. Generalis[2], and Tomoaki Itano[3]

(Received December 5, 2020)

Abstract

Spiral states are commonly observed in pattern formation on a sphere. Li et al.(Phys. Rev. E, Vol. 71, 016301 [2005]) previously proposed a method to generate the spiral states by adopting mixed modes with adjacent wavenumbers like $l = l_0, l_0 + 1$, as the initial condition of a time-developing numerical simulation. Herein, using the Swift-Hohenberg equation as an example, we show that Li's empirical method can be successful only in particular regions of parameter space. Tracing the state by a continuation method generated from the static state via three symmetry breakings, the spiral state may be regarded as a resonant state generated by the combination of a few degenerate unstable modes with different azimuthal wave numbers.

1. Introduction

Pattern formation on spherical geometry is observed in both physical and biological phenomena [1]. Thermal convection driven in the earth's outer core is an example of spherical pattern formation that is potentially significant to human life via the influence of the geomagnetic field [2]. In biological applications, the morphogenesis of tumours, viruses, and embryos may be formulated in the context of a reaction-diffusion system, as in the case of thermal convection. In general, subject to the isotropy (spherically homogeneous) condition, the set of equations governing these systems should be invariant against coordinate rotation. Therefore, inherent in the system, several unstable modes arise at the onset of the instability of the conductive state with an increase in control parameters. Based on the linear stability analysis of such an isotropic system, the unstable modes at the onset of the instability must be associated with the degenerated spherical harmonics, $Y_l^m(\theta, \phi)$, as sinusoidal waves for the planar homogeneous system. Thus, the $2l + 1$ degenerated unstable modes may emerge simultaneously so that a nontrivial balance between the linear growth of the unstable modes and the relaxation of viscous diffusion will generate either a stable or unstable equilibrium state via nonlinear mode interaction. As a result, the generated equilibrium state satisfies either axisymmetric, tetrahedral, cubic-octahedral, or dodecahedral-icosahedral symmetry [3].

To date, it was intuitively believed that such highly symmetric steady states would be superior to either other less symmetric equilibria or asymmetric chaotic states in the transitional stage. Recent numerical studies [4], however, have reported that, at the onset of the instability, a less-symmetric equilibrium state, namely, a *single-arm spiral roll state*, coexists with other highly symmetric equilibrium states and appears to be stable. Fig. 1 shows an isothermal surface of a spiral state realised in a thermal convective system between

[1] Graduate School of Science and Engineering, Kansai University, Osaka, Japan
[2] College of Engineering and Applied Sciences, Department of Mathematics, Aston University, Birmingham, United Kingdom
[3] Department of Pure and Applied Physics, Faculty of Engineering Science, Kansai University, Osaka, 564-8680, Japan

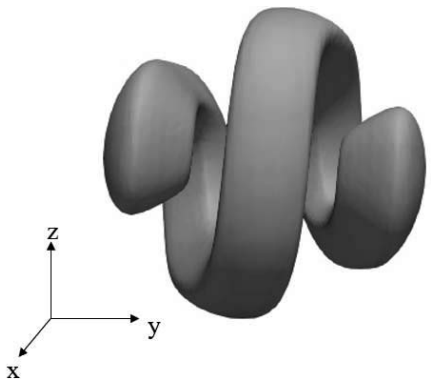

Fig. 1. A spiral state obtained at $r_{\rm in}/r_{\rm out} = 0.5$ near the critical Rayleigh number is visualised by an isosurface of the thermal deviation from the mean temperature.

doubly concentric spherical boundaries, and Fig. 2 shows its contour plot projected in the $\theta - \phi$ plane. Li et al. [5] pointed out that the spiral states may be generated by adopting a mixed-mode combination with adjacent azimuthal wave numbers like $l = l_0$ and $l_0 + 1$ as the initial condition of transient simulations. They suggested that this initial condition may lead to the spiral state at the parameters, where linear growth rates of both $Y_{l_0}^{m_1}$ and $Y_{l_0+1}^{m_2}$ ($|m_1| < l_0$ and $|m_2| < l_0 + 1$) become positive simultaneously [6] via a nontrivial balance of the mode weight functions. In the recent numerical study on the spherical Rayleigh-Bénard convective system [7], it has also been confirmed that the spiral state is not steady and that the parameter range in which the solution exists is relatively restricted. Bearing in mind that a small amount of randomness of symmetry breaking in the initial condition is common in nature, such a less symmetric state, possibly preferred by the system, might have been worth exploring further. In the present study, we adopt the Swift-Hohenberg equation as a model equation to understand some of the unexpected aspects of this particular state that have hitherto remained obscure. In this study, we define the spiral state as follows. First, one isosurface is visualised at a certain threshold, and is path-connected in the sense of topology. Second, the spiral state is not equivalent to a torus of topology. Strictly speaking, the spiral pattern should be defined by resorting to the symmetries illustrated in Fig. 5.

2. Formulation

We consider a time-dependent complex order function $f(t, \theta, \phi)$ with $0 \le \theta \le \pi$, $0 \le \phi < 2\pi$ that obeys the Swift-Hohenberg equation [8] without a quadratic term:

$$\frac{\partial f}{\partial t} = [\alpha - (1 + \nabla^2)^2]f - f^3 =: F(f) \quad , \tag{1}$$

on a sphere of radius R, where α is the bifurcation control parameter. Let us take the case of the thick spherical shell as an example. Assuming that the velocity and temperature fields are

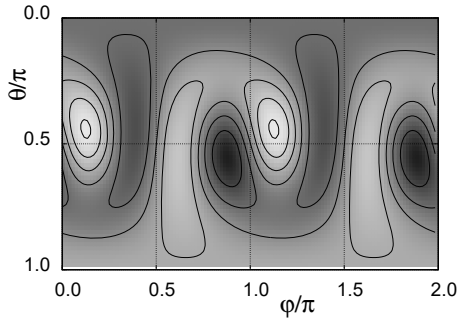

Fig. 2. The contour plot of the spiral state at $r = \frac{1}{2}(r_{\rm in} + r_{\rm out})$ shown in the Fig. 1 is expanded in $\theta - \phi$ plane. θ is the angle to the positive z-axis and ϕ is the angle to the positive x-axis. The darker the colour, the cooler the temperature.

governed by the principal equation of Rayleigh-Bénard convection in spherical geometry and are approximated as $\sin\left(\pi\frac{r-r_{\rm in}}{r_{\rm out}-r_{\rm in}}\right)+\mathrm{O}(f^2)$, the equation of the order parameter, $f(r,\theta,\phi,t)$, may be described qualitatively by Eq. (1).

The spherical periodic boundary condition restricts the variety of the global patterns. Recently, Eq. (1) was utilised to find candidate solutions to Kelvin's problem on minimal surfaces. According to [9], the normalized energy $\mathcal{E}$ associated with the equation may be defined as

$$\mathcal{E}(f) := \frac{1}{4\pi}\int\Big(-\frac{\alpha}{2}f^2 + \frac{1}{2}[(\boldsymbol{\nabla}^2+1)f]^2 + \frac{1}{4}f^4\Big)d\Omega \quad .$$

It should be noted that $\dfrac{d\mathcal{E}}{dt} = -\dfrac{1}{4\pi}\displaystyle\int(\frac{\partial f}{\partial t})^2 d\Omega \leq 0$, so that an equilibrium state achieved by integration must be a certain steady state, which corresponds to a local minimum of the energy in the functional space. The eigenvalue problem can be constituted from the linearisation of the equation under the spherical periodic boundary condition with growth rate, σ, being the corresponding eigenvalue. The sign of $\sigma = \alpha - (1 - \dfrac{l(l+1)}{R^2})^2$ determines the linear stability on the static state ($f = 0$) against the infinitesimal disturbance of eigenfunction, which is a combination of the spherical harmonics $Y_l^m(\theta,\phi)$. Thus, we define the critical growth rate as:

$$\alpha_{cr}(l,R) := \Big(1 - \frac{l(l+1)}{R^2}\Big)^2 \quad .$$

In other words, the static state at (R,α) may be unstable against multiple Y_l^ms with (l,m), that satisfy $\alpha_{cr}(l,R) < \alpha$ (see Fig. 3).

Taking the governing equation as a set of simultaneous differential equations for $f_{l,m}$, the time development of the state was calculated using the Runge-Kutta method, with the aid of the numerical library on spherical harmonics [10, 11] utilising the Gauss-Lobatto collocation method. Generally speaking, the time-varying scalar field on the sphere is written as the superposition of spherical harmonics,

$$f(\theta,\phi) = \sum_{l,m} f_{l,m}(t) Y_l^m(\theta,\phi) \ ,$$

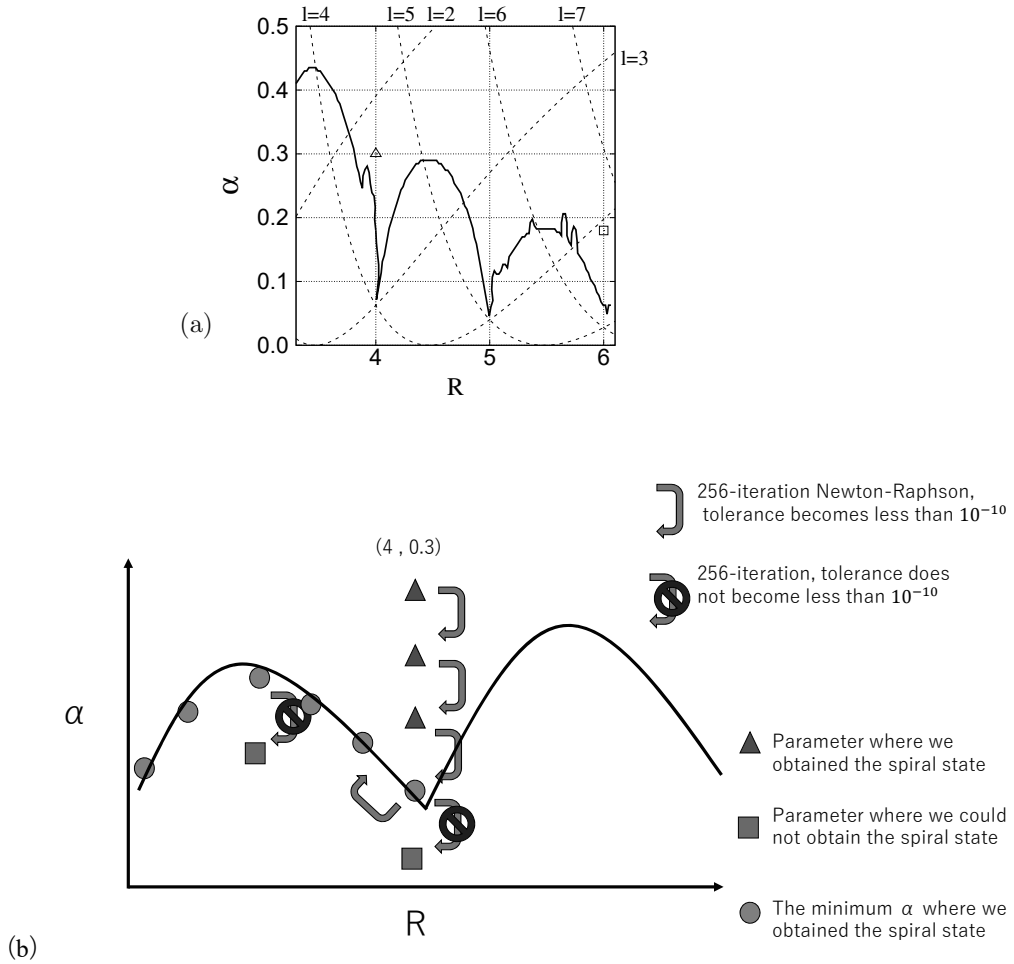

Fig. 3. (a) Neutral curves of the static state, $\alpha = \alpha_l(R)$, on which the static state is neutral to a disturbance of the l-th degree spherical harmonic functions, are indicated as dashed curves with different l. Thus, for a fixed value of R, the static state is asymptotically stable against any infinitesimal disturbance at $\alpha < \alpha_{\min}(R) := \min\{\alpha_{\rm cr}(l,R); l = 1, 2, \cdots\}$, and otherwise unstable. The triangle symbol plotted at $(R, \alpha) = (4, 0.3)$ indicates the parameters, where a steady single-arm spiral state was obtained numerically by the Newton-Raphson scheme. A spiral state can be numerically found above the solid curve. (b) The second figure schematically depicts the procedure undertaken to obtain the nonlinear spiral states.

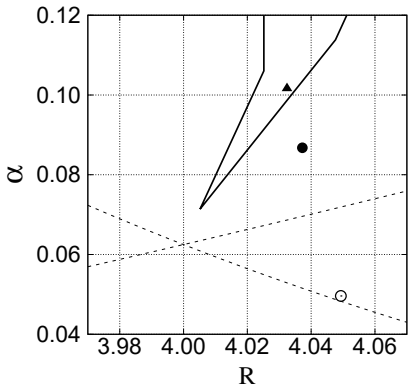

Fig. 4. Enlarged figure of the range of $3.98 < R < 4.06, 0.04 < \alpha < 0.12$ in Fig. 3

with, in general, time dependent weight functions $f_{l,m}(t)$.

We employ the Newton-Raphson method to numerically identify the steady state $f_{\rm s}$ satisfying $F(f_{\rm s}) = 0$ in Eq. (1). Here, we refer to the n-th approximated state as $f^{(n)}$ $(n = 0, 1, \cdots)$. Assuming that $f^{(n)}$ is sufficiently close to the solution $f_{\rm s}$, the Taylor expansion of F around $f = f^{(n)}$ is $F(f_{\rm s}) = F(f^{(n)}) + F'(f^{(n)})(f_{\rm s} - f^{(n)}) + {\rm O}(|f^{(n)} - f_{\rm s}|^2)$, where $F(f_{\rm s})$ and the higher order term can be regarded as zero. Symbolically replacing $f^{(n)} - f_{\rm s}$ with Δf, F' by the Jacobian matrix A, and $F(f^{(n)})$ by b, the method is equivalent to algebraically solving $A\Delta f = -b$ to obtain $f^{(n+1)}$ and then replacing $f^{(n+1)}$ to $f^{(n)}$ iteratively. Expecting that $|F(f^{(n)})| < |F(f^{(n)}|$, we obtain $f_{\rm s}$ from $F(f^{(n)}) \to 0$ within a tolerance factor.

3. Methodology

Since f is a real valued function, $f_{l,-m} = f^*_{l,m}$ is satisfied, with $f_{l,0}$ as purely real. Eq. (1) is invariant with respect to rotations SO3 of the coordinate system as well as the reflection $f \to -f$, since Eq. (1) is constituted only by linear and cubic terms. The calculations are simplified by taking into account the symmetry satisfied by the spiral state, $f(\pi - \theta, -\phi) = -f(\theta, \phi)$ and $f(\theta, \pi + \phi) = f(\theta, \phi)$. While the former is termed as the parity symmetry on the x-axis, which fixes the phase of the spiral state around the z-axis to locate the tips of the spiral arm on the x-axis, the latter is the two-fold symmetry of the spiral state on the z-axis. The parity and two-fold symmetries are equivalent to $f^*_{l,m} = (-1)^l f_{l,m}$ and $f_{l,m} = (-1)^m f_{l,m}$, respectively. These symmetries are followed by an alternative symmetry $f(\theta, \frac{\pi}{2} - \phi) = -f(\pi - \theta, \frac{\pi}{2} + \phi)$ that is automatically satisfied, which may be termed as the parity symmetry on the y-axis.

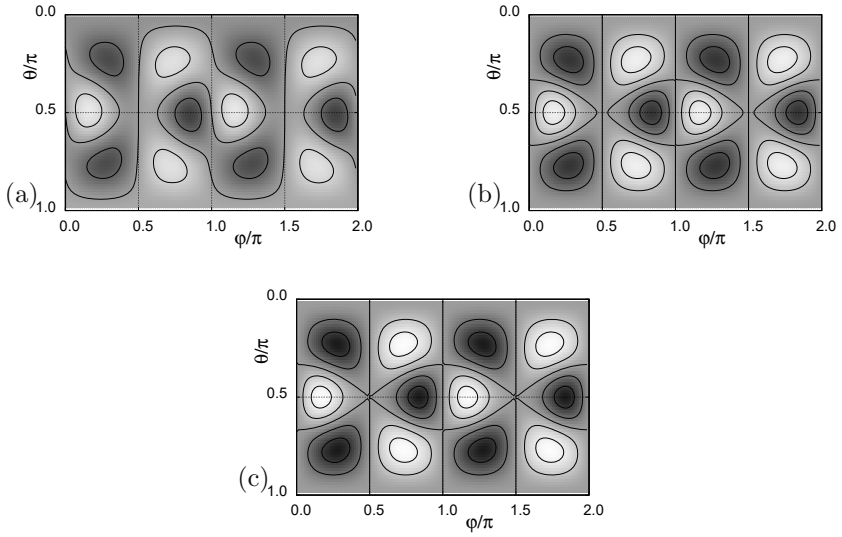

Fig. 5. (a) $(R, \alpha) = (4.05, 0.05)$, (b) $(R, \alpha) = (4.04, 0.09)$, and (c) $(R, \alpha) = (4.03, 0.10)$, correspond to the filled triangle, filled circle, and open circle symbols in Fig. 4, respectively.

4. Results

We have obtained some spiral state candidates from the numerical simulation at $(R, \alpha) = (4, 0.3)$. One of them was numerically obtained using the Newton-Raphson techniques subject to the symmetries explained above, which are indicated by the open triangle symbol in Fig. 3. Adopting this spiral state as a seed, the Newton-Raphson method allowed us to adiabatically trace the spiral state in the parameter space, step by step by increasing or decreasing the values of these parameters (R, α). The thick solid curve in the figure is a boundary, out of which a seed used by Newton-Raphson does not converge to the spiral state in 256 iterations. The procedure to obtain this boundary curve is as follows: (1) We traced the spiral state by decreasing α sequentially from the converged spiral state at the open triangle symbol of Fig. 4, (2) We determined the $(i+1)$-th parameter (R_{i+1}, α_{i+1}) for the unsolved spiral state to be $(R_i + \Delta R, \alpha_i + \Delta\alpha)$ from the i-th parameter (R_i, α_i) for the solved spiral state. Here, ΔR and $\Delta\alpha$ are both small values $O(10^{-3})$. (3) We iterated using the Newton-Raphson method, unless the calculation converges within 256 iterations. Next, some changes $(\Delta R, \Delta\alpha)$ were introduced towards the left-hand (or right-hand) turning direction by a small angle, (4) We increased i and returned to the second step of our process. The algorithm is similar to a person trying to move forward in the dark with his right (or left) hand continuously touching the wall.

The shape of the boundary above the spiral state that can be numerically found is like a series of bumpy mountains. It should be noted that a valley of adjacent mountains is close to intersections of neutral curves with a couple of adjacent azimuthal wave numbers, for example $l = 3, 4$ or $l = 4, 5$, where the spiral state could be obtained at relatively low

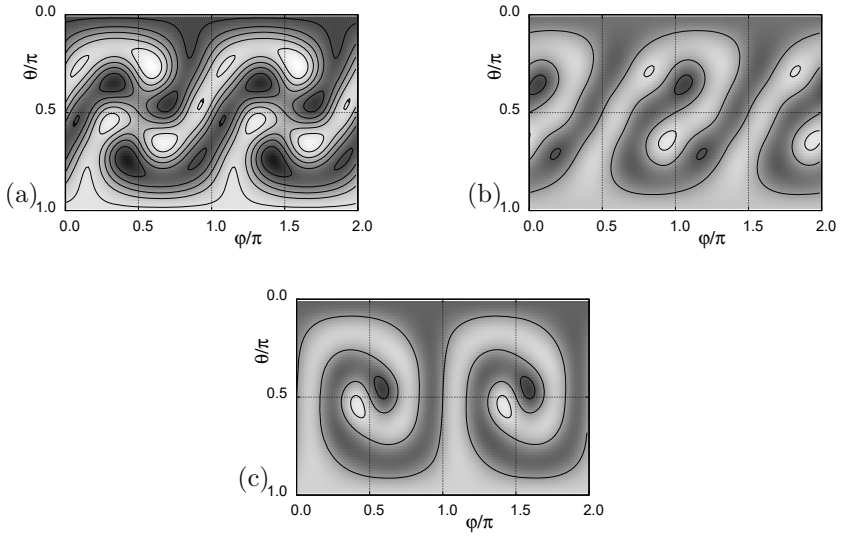

Fig. 6. Different spiral states converged at $(R, \alpha) = (6, 0.18)$ (open square symbol in Fig. 3).

α without difficulty. In other words, the spiral state may have its bifurcation origin at the intersections of neutral curves by adopting a mixed-mode combination with adjacent azimuthal wave numbers. This is reminiscent of the fact that, previously, the spiral states could be generated by adopting mixed modes with adjacent wave numbers $l = l_0, l_0 + 1$ as the initial condition of the time-developing numerical simulation [5].

Fig. 4 shows that the corner of the boundary approaches the intersection of the neutral curves with adjacent azimuthal wave numbers, $l = 3$ and 4. We investigated the details of the bifurcation behaviour of the spiral state around the origin as follows. Adopting the spiral state obtained at $(R, \alpha) = (4.03, 0.102)$ (indicated by the filled triangle symbol) as a seed, we obtained the two converged states at $(R, \alpha) = (4.04, 0.087)$ and $(4.05, 0.050)$, as indicated by the filled circle and the open circle in the figure. The contour plots of the first, second, and third states are illustrated in Fig. 5(a), (b), and (c), respectively. The first state (filled triangle symbol) satisfies only the parity symmetry with respect to the x-axis and the twofold symmetry with respect to the z-axis. The second state (filled circle symbol) satisfies not only these two symmetries but also another independent symmetry, namely, the anti-reflection symmetry on the x-z plane, $f(\theta, \phi) = -f(\theta, -\phi)$, as illustrated in Fig. 5(b). The third state (open circle symbol) satisfies not only these three symmetries but also another independent symmetry, namely, the threefold symmetry with respect to the y-axis. Note that the y-axis corresponds to $(\frac{\phi}{\pi}, \frac{\theta}{\pi}) = (0.5,0.5)$ or $(1.5,0.5)$. Thus, the spiral state may generate from the static state via three symmetry breakings.

5. Concluding remarks

It is known that spiral states are commonly observed in pattern formation on a sphere. Using

the Swift-Hohenberg equation, we showed that Li's empirical method can be successful only in particular regions of parameter space. The spiral state in pattern formation in spherical geometry may be considered as a resonance generated by a few degenerated unstable modes with different azimuthal wavenumbers [12, 13].

Here, we present an example of a low-dimensional dynamical model in that an equilibrium state bifurcates from the degenerated unstable modes. Provided that a dynamical system $(x(t), y(t))$ obeys $\dot{x} = (\alpha - R)x - x^3$, $\dot{y} = (\alpha - R)y - y^3$, the equilibrium state of the system that produces the stable resonant state is given as $(x, y) = (\pm\sqrt{\alpha - R}, \pm\sqrt{\alpha - (1 - R)})$ for both $R < \alpha$ and $1 - R < \alpha$. Originating at the intersection of the neutral lines $\alpha = R$ and $\alpha = 1 - R$, this state extends in a delta area between the lines.

We confirmed that several different spiral states coexist at the parameter $(R, \alpha) = (6.0, 0.18)$. The initial condition of $f_{l,m}(t)$ selects one of the three patterns. The obtained spiral states are illustrated as a contour plot in Fig. 6. It should be noted that each spiral state may have a different range of existence in parameter space; in other words, there are multiple boundaries described as solid curves in Fig. 3 for every spiral state.

This work has been supported in part by KAKENHI (20K04294). The work was also supported by the European Union Horizon 2020 Research Innovation and Staff Exchange (RISE) programme ATM2BT, grant number 824022, for which Kansai University is part of.

[1] P. C. Matthews. Pattern formation on a sphere. Phys Rev E, 67(3):036206, 2003.
[2] C. M. R. Fowler. The solid earth, 2004.
[3] F. H. Busse. Patterns of convection in spherical shells. J Fluid Mech, 72(1):67–85, 1975.
[4] P. Zhang, K. Liao, and K. Zhang. Patterns in spherical rayleigh-bénard convection: A giant spiral roll and its dislocations. Phys Rev E, 66:055203(R), 2002.
[5] L. Li, P. Zhang, X. Liao, and K. Zhang. Multiplicity of nonlinear thermal convection in a spherical shell. Phys Rev E, 71:016301, 2005.
[6] S. Rachel and P. Matthews. Symmetric spiral patterns on spheres. SIAM J. Applied Dynamical Systems, 10(3):1177–1211, 2011.
[7] T. Itano, T. Ninomiya, K. Konno, and M. Sugihara-Seki. J. Phys. Soc. Jpn, 84:103401, 2015.
[8] J. B. Swift and P.C. Hohenberg. Hydrodynamic fluctuations at the convective instability. Phys Rev A, 15:319–328, 1977.
[9] R. Gabbrielli. A new counter-example to kelvin's conjecture on minimal surfaces. Philosophical Magazine Letters, 89:483–491, 2009.
[10] N. Schaeffer. Efficient spherical harmonic transforms aimed at pseudospectral numerical simulations. Geochemistry, Geophysics, Geosystems, 14(3):751–758, 2013.
[11] M. Frigo and S. G. Johnson. The design and implementation of FFTW3. Proceedings of the IEEE, 93(2):216–231, 2005. Special issue on "Program Generation, Optimization, and Platf orm Adaptation".
[12] T. Akinaga, T. Itano, and S. Generalis. Symmetry breaking perturbative flows to retrieve resonant modes in plane shear layers. Arxiv preprint flu-dyn http://arxiv.org/abs/1503.02625, 2015.
[13] T. Akinaga, T. Itano, and S. Generalis. Convection induced by instabilities in the presence of a transverse seepage. Chaos, Solitons and Fractals, 91:533–543, 2016.